COMPOSITION AND SIZE OF MARTIAN AEROSOLS AS SEEN BY NOMAD-SO DURING MY34 & 35.

Aurélien Stolzenbach, *Instituo de Astrofísica de Andalucia, Granada, Spain (astolzenba@iaa.es)*, **Miguel-Angel López Valverde, Adrian Brines, Ashimananda Modak, Bern Funke, Francisco González-Galindo,** *Instituo de Astrofísica de Andalucia, Granada, Spain*, **Ian Thomas,** *Belgian Royal Institute for Space Aeronomy, Brussels, Belgium*, **Giuliano Liuzzi, Geronimo Villanueva,** *NASA Goddard Space Flight Center, USA*, **Mikhail Luginin,** *Space Research Institute (IKI), Moscow, Russia*, **Shohei Aoki,** *University of Tokyo, Kashiwa, Japan*.

Introduction

Climates on all planets are heavily influenced by aerosols in their atmospheres. Their nature, size's distribution and content affect the energy budget, hence the atmospheric dynamic of the planet. On Mars, we know that three types of aerosol exist. Dust, water ice and carbon dioxide ice. Dust mainly affects the thermal structure of the martian atmosphere through radiative heating [1]. Water ice has a broader effect since it impacts the thermal structure, as for dust, through modifying the radiative equilibrium [2] but also the martian water cycle [3]. Carbon dioxide ice condensation occurs mainly close to the poles during winter or at high altitudes [4]. Water and carbon dioxide ice also influence dust content and size distribution through their condensation onto smaller dust particles acting as condensation nuclei [5].

ExoMars TGO mission (ESA/Roscosmos) was primarily designed to study trace gases, thermal structure and aerosol content in Mars atmosphere with unprecedented vertical resolution [6]. Previous study by [7] retrieved dust and water ice particle size and abundances from an inversion method using NOMAD-SO data. Their work used a fixed effective variance but provided meaningful insight on the challenges about simultaneously retrieving information about dust and water ice from NOMAD-SO observations. Moreover, [7] demonstrated the sharp gradient of the water ice effective radius in the troposphere and its diurnal variability.

NOMAD-SO Data processing

NOMAD (Nadir and Occultation for MArs Discovery) is suite of two infrared spectrometers onboard the ExoMars 2016 Trace Gas Orbiter (TGO) orbiter, covering the spectral range of 0.2 to $4.3\,\mu\mathrm{m}$ [8]. The instrument has three spectral channels in order to observe the Martian atmosphere in nadir, limb or solar occultation geometries at different wavelengths. Two IR spectrometers composed by the Solar Occultation channel (SO), operating in the range between 2.3 to $4.3\,\mu\mathrm{m}$ (2320-$4350\,\mathrm{cm}^{-1}$) and the Limb Nadir Occultation channel (LNO) and a third one operating in the UV-visible (UVIS), capable of both nadir and occultation observations. The SO channel has been designed similar to the Solar Occultation in the Infrared (SOIR) instrument onboard *Venus Express*. It uses an echelle grating with a density of ≈ 4 lines/mm in a Litrow configuration. An Acousto-Optical Tunable Filter (AOTF) is used to select different spectral windows (with a width that varies from 20 to $35\,\mathrm{cm}^{-1}$). Each window corresponds to the desired diffraction order to be used during the atmospheric scan. The spectral resolution of the SO channel is $\lambda/\Delta\lambda = 20000$. The sampling of this channel is approximately of 1 second, allowing a vertical sampling about 1km. The AOTF also permits a quick change between diffraction orders. As a result, the SO channel is able to observe the atmosphere at a given altitude with 6 different diffraction every second.

For this study, we selected a configuration of 5 diffraction orders (121,134,149,168,190) spanning the overall spectral range of NOMAD. These orders are selected because they are regularly used together in a large fraction of NOMAD solar occultation observations during the first year of the mission. They also cover a broad spectral range, essential for a good characterization of the aerosol composition. Our dataset covers a full martian year starting at MY 34 L_S 180° and ends at the same L_S of MY 35. It represents 563 vertical scans with the 5 order selected present in each one.

We are using the level 1 transmittances spectrum provided by the PI team at the Belgian Royal Institute of Spatial Aeronomy (BIRA). These calibrated transmittance needs to be furthermore processed to correct residual continuum effects and frequency shifts. The four prominent features to be taken into account in what we refer to "Pre-Processing phase" are the Instrument Line Shape (ILS), the AOTF response, a signal spectral shift and continuum bending. At the IAA, we developped an in-house preprocessing program that evaluates the latter two features, the spectral shift and continuum bending. To do so, we are using a radiative forward model named KOPRA (Karlsruhe Optimized Radiative transfer Algorithm described in [9]). The reference atmosphere is taken from the LMDZ Mars GCM [10] for an exact location and season as the NOMAD data. The radiative transfer forward model KOPRA uses HITRAN 2016 spectral lines absorption data for relevant gases in each order (CO_2, CO and H_2O mainly).

BIRA, Goddard and IAA teams worked at a common solution for the ILS and AOTF. The AOTF updated calibration presented in [11] describe the AOTF response

with an asymmetric sinc function added to a Gaussian, operating as an offset. The parameters that describe the AOTF are wavenumber dependent. The ILS can be described by an addition of two Gaussian functions with a separation and a scaling ratio between them that varies across the diffraction orders.

In order to evluate the local extinction due to aerosols, we use an inversion program called RCP. it stands for Retrieval Control Program and is a multi-parameter non-linear least squares fitting of measured and modeled spectra [12]. The forward model, KOPRA, was recently adapted to limb emissions on Mars [13] and for this work it has been adapted to solar occultation data on Mars for the first time, and in particular to the NOMAD SO channel with implementation of the asymmetric AOTF transfer function and the double Gaussian ILS. Regarding the aerosols, the first guess and a priori are always a null vertical profile of the extinction. RCP solves iteratively the inverse problem [14] and is described in details in [15]. The calculation of the model spectra and Jacobians is performed with KOPRA, being called in each step of the iteration. The measurement covariance matrix is calculated from the noise-equivalent spectral radiance provided with the NOMAD level 1a data. The regularization matrix is build from Tikhonov-type terms of different orders which can be combined to obtain a custom-tailored regularization for any particular retrieval problem. RCP uses a Levenberg-Marquardt damping which is forced to be zero in the last iteration. Convergence is reached when the change of the retrieval parameters with respect to the previous iteration is smaller than a certain fraction of the expected noise retrieval error. For this study on martian aerosol we decided to select a regularization profile that deals with the trade-off between very oscillating extinction vertical profile with higher vertical resolution and a very smooth extinction vertical profile with lower vertical resolution. A example of the extinction profile is shown in fig. 1. The retrieved extinctions differs from the usual evaluation using the Onion-peeling or Abel's transform method since with this global fit we have other key parameters as the averaging kernel and the vertical resolution. This is an important difference with the previous work on aerosols using ACS data [16, 17], who used an onion peeling inversion.

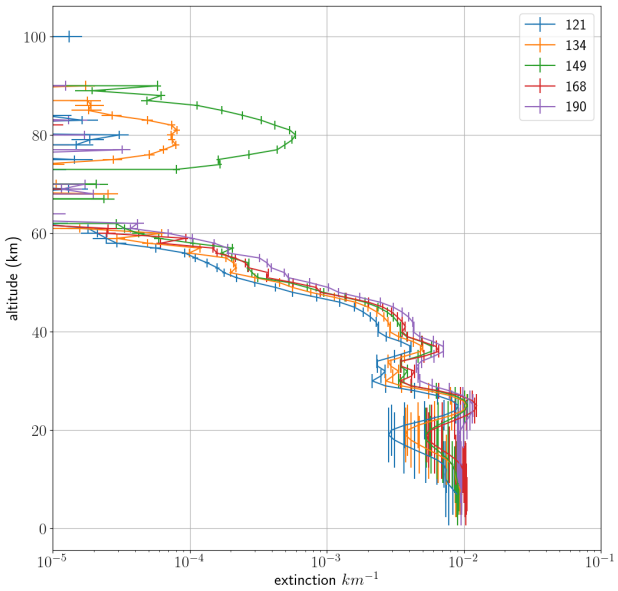

Figure 1: Retrieved extinction vertical profiles from orbit 20180625_050514_1p0a_SO_A_E. the absolute error of the extinction is plotted horizontally and the vertical resolution vertically at each altitude point.

Mean extinction cross-section ratio modelling

In order to model the optical behavior of the Martian aerosol we need to model first its size distribution. We chose the log-normal distribution, as shown below, which is widely used in atmospheric sciences.

$$n_{\mathrm{N}}(\mathrm{r}) = \frac{\mathrm{N}}{\sqrt{2\pi}\,\mathrm{r}\,\ln(\sigma_g)} \cdot \exp\left(-\frac{(\ln(\mathrm{r}) - \ln(\bar{\mathrm{r}}_g))^2}{2\ln(\sigma_g)^2}\right)$$

The log-normal distribution is a function of two parameters $(\bar{\mathrm{r}}_g, \sigma_g)$. In optics, we usually change those parameters to more suitable ones. The effective radius, r_{eff}, which represents the ability of the size distribution to remove a part of the incoming light beam, and its corresponding effective variance ν_{eff}.

For any aerosol size distribution, the extinction k at a wavelength λ is defined as follow:

$$k(\lambda) = \mathrm{N}\,\sigma_{ext}(\lambda, \mathrm{r}_{eff}, \nu_{eff}) \tag{1}$$

Where k is the extinction in km^{-1}, N the aerosol number density and $\sigma_{\mathrm{ext}}(\lambda)$ is the mean average extinction cross-section at a wavelength λ and for a specific aerosol distribution defined by the two parameters $(\mathrm{r}_{eff}, \nu_{eff})$. In order to get rid of the number density N, we can construct a new variable χ defined as follow:

$$\chi(\lambda) = \frac{k(\lambda)}{k(\lambda_0)} \tag{2}$$

On Mars, the aerosol distribution exhibits a bimodal behavior as shown by [18]. In order to model this characteristic of martian aerosol, we define an extinction ratio χ_m (eq. (3)) for a mixture of dust and water ice as done in [16]. In eq. (3), the subscript d is for dust and wi is for water ice. The term γ is the ratio of the number densities of water ice over dust, N_{wi}/N_d

$$\chi_m(\lambda) = \frac{k_d(\lambda) + \gamma\, k_{wi}(\lambda)}{k_d(\lambda_0) + \gamma\, k_{wi}(\lambda_0)} \tag{3}$$

Using evaluated refractive indexes for Dust, using [19], and water ice,using [20, 21], we run a Lorenz-Mie code for polydisperse spherical particle from [22] for a set of (r_{eff}, ν_{eff}) in order to evaluate the mean average extinction cross-section at the selected NOMAD order's wavelengths.

Aerosol composition and size distribution evaluation

We are using a mix of non-linear least square and brute force to evaluate the best set of parameters (r_{eff} , ν_{eff} ,γ), for pure dust, pure H_2O ice and a mixture of the two represented by γ. The non-linear least square algorithm is provided by the SciPy Python package [23]. We have selected the Trust Region Reflective (TRF) algorithm as solver [24, 25] instead of the traditional Levenberg-Marquandt since the TRF solver handles better boundary conditions. we filter for low averaging kernel, low effective variance, bad merit function and high vertical resolution.

The errors associated with every parameters are selected at the appropriate step by the diagonal component of the covariance matrix provided by the NLSQ algorithm. Since the retrieved extinction provided by the global fit of RCP have very low errors, we are confident that results with a merit function below 10 are still relevant. To assess the robustness of our fitting procedure, we will present results against synthetic extinction ratios signal

Short overview of the results

The MY 34 GDS reached a planetary scale at $L_S \approx 195°$. Our detection of dust and water ice aerosols reached altitudes up to $90\,\mathrm{km}$ in both hemisphere. The lower deck of aerosol, with water ice particle size of a few microns and dust particle size close to $1\,\mu\mathrm{m}$, rise up to $35\,\mathrm{km}$ in both hemisphere.

In both hemisphere, starting at $L_S = 210°$, we can see the decay of the GDS starting from the poles. The amount of aerosol does not rise up more than $30\,\mathrm{km}$. [7] showed a similar lack of water ice and dust content for the same location and period. Unfortunately, we do not have results from ACS for this period and location [16]. Still in the northern hemisphere around $L_S = 240°$, we observe an increase of the size of water ice particles above 45 to $60\,\mathrm{km}$. This increase is due to mid to low latitudes measurements at similar L_S, also observed by [7]. The result on the size of the water ice particles in fig. 2 shows water ice $\bar{r}_g$ goes from small sub-micron values ($< 0.5\,\mu\mathrm{m}$) to sizes in the range of a few $\mu\mathrm{m}$. A similar result was already observed by [7] but with an effective radius greater than $4\,\mu\mathrm{m}$ for altitudes above $\approx 40\,\mathrm{km}$. This vertical behavior of the water ice particle size was attributed to strong convective dust storms, called "rocket dust storms", characteristic of this season and location [26].

An inter-annual C-type dust storm [27, 28] occurs every martian year around $L_S = 320°$. Top level altitudes for water ice and dust aerosol are close to $95\,\mathrm{km}$. Both their sizes stay in their global ranges, with sub-micron particles for water ice and a decreasing size, from micron to sub-micron, with altitude for dust. This C-type storm event in MY 34 ends before $L_S = 330°$.

We will present in much details about other parameters such as r_{eff} , ν_{eff} ,and the mass loading. We will also talk about the inherent bias of our retrieval scheme and its impact on the results.

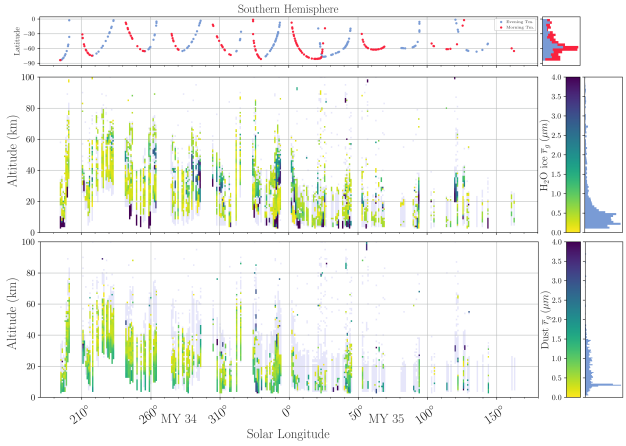

Figure 2: Median radius $\bar{r}_g$ results of the aerosol distribution properties analysis scheme in the southern hemisphere. The filtered aerosol fitting points due to bad merit function or low/high effective variance are shown in light grey.

References

[1] Donald W. Davies. “Effects of dust on the heating of Mars’ Surface and atmosphere”. en. In: *Journal of Geophysical Research: Solid Earth* 84.B14 (1979), pp. 8289–8293.

[2] J.-B. Madeleine et al. “Aphelion water-ice cloud mapping and property retrieval using the OMEGA imaging spectrometer onboard Mars Express”. en. In: *Journal of Geophysical Research: Planets* 117.E11 (2012).

[3] F. Montmessin et al. “Origin and role of water ice clouds in the Martian water cycle as inferred from a general circulation model”. en. In: *Journal of Geophysical Research: Planets* 109.E10 (2004).

[4] R. Todd Clancy et al. “Mars Clouds”. In: *The Atmosphere and Climate of Mars*. Ed. by François Forget et al. Cambridge Planetary Science. Cambridge: Cambridge University Press, 2017, pp. 76–105.

[5] T. Navarro, F. Forget, E. Millour, and S. J. Greybush. “Detection of detached dust layers in the Martian atmosphere from their thermal signature using assimilation”. en. In: *Geophysical Research Letters* 41.19 (2014), pp. 6620–6626.

[6] J. Vago et al. “ESA ExoMars program: The next step in exploring Mars”. en. In: *Solar System Research* 49.7 (Dec. 2015), pp. 518–528.

[7] Giuliano Liuzzi et al. “Strong Variability of Martian Water Ice Clouds During Dust Storms Revealed From ExoMars Trace Gas Orbiter/NOMAD”. en. In: *Journal of Geophysical Research: Planets* 125.4 (2020).

[8] A. C. Vandaele et al. “NOMAD, an Integrated Suite of Three Spectrometers for the ExoMars Trace Gas Mission: Technical Description, Science Objectives and Expected Performance”. en. In: *Space Science Reviews* 214.5 (June 2018), p. 80.

[9] Gabriele P. Stiller et al. “Karlsruhe optimized and precise radiative transfer algorithm: I. Requirements, justification, and model error estimation”. In: *Optical Remote Sensing of the Atmosphere and Clouds*. Ed. by Jinxue Wang, Beiying Wu, Toshihiro Ogawa, and Zhenghua Guan. Vol. 3501. International Society for Optics and Photonics. SPIE, 1998, pp. 257–268.

[10] François Forget et al. “Improved general circulation models of the Martian atmosphere from the surface to above 80 km”. In: *Journal of Geophysical Research: Planets* 104.E10 (1999), pp. 24155–24175.

[11] Geronimo L Villanueva et al. “The deuterium isotopic ratio of water released from the Martian caps as measured with TGO/NOMAD”. In: *GRL* (2022).

[12] T. von Clarmann et al. “Retrieval of temperature and tangent altitude pointing from limb emission spectra recorded from space by the Michelson Interferometer for Passive Atmospheric Sounding (MIPAS)”. en. In: *Journal of Geophysical Research: Atmospheres* 108.D23 (2003).

[13] Sergio Jiménez-Monferrer et al. “CO2 retrievals in the Mars daylight thermosphere from its 4.3μm limb emission measured by OMEGA/MEx”. In: *Icarus* 353 (2021), p. 113830.

[14] Clive D Rodgers. *Inverse Methods for Atmospheric Sounding*. WORLD SCIENTIFIC, 2000.

[15] Jurado Navarro and Angel Aythami. *Retrieval of CO2 and collisional parameters from the MIPAS spectra in the earth atmosphere*. eng. Universidad de Granada, 2016.

[16] M. Luginin et al. “Properties of Water Ice and Dust Particles in the Atmosphere of Mars During the 2018 Global Dust Storm as Inferred From the Atmospheric Chemistry Suite”. en. In: *Journal of Geophysical Research: Planets* 125.11 (2020), e2020JE006419.

[17] A. Stcherbinine et al. “Martian Water Ice Clouds During the 2018 Global Dust Storm as Observed by the ACS-MIR Channel Onboard the Trace Gas Orbiter”. en. In: *Journal of Geophysical Research: Planets* 125.3 (2020), e2019JE006300.

[18] A. A. Fedorova et al. “Evidence for a bimodal size distribution for the suspended aerosol particles on Mars”. en. In: *Icarus* 231 (Mar. 2014), pp. 239–260.

[19] M. J. Wolff et al. “Wavelength dependence of dust aerosol single scattering albedo as observed by the Compact Reconnaissance Imaging Spectrometer”. en. In: *Journal of Geophysical Research: Planets* 114.E2 (2009).

[20] Stephen G. Warren and Richard E. Brandt. “Optical constants of ice from the ultraviolet to the microwave: A revised compilation”. en. In: *Journal of Geophysical Research: Atmospheres* 113.D14 (2008).

[21] M. L. Clapp, D. R. Worsnop, and R. E. Miller. “Frequency-dependent optical constants of water ice obtained directly from aerosol extinction spectra”. In: *The Journal of Physical Chemistry* 99.17 (Apr. 1995), pp. 6317–6326.

[22] Michael I Mishchenko, Larry D Travis, and Andrew A Lacis. *Scattering, absorption, and emission of light by small particles*. Cambridge university press, 2002.

[23] Pauli Virtanen et al. “SciPy 1.0: Fundamental Algorithms for Scientific Computing in Python”. In: *Nature Methods* 17 (2020), pp. 261–272.

[24] D. C. Sorensen. “Newton’s Method with a Model Trust Region Modification”. In: *SIAM Journal on Numerical Analysis* 19.2 (Apr. 1982), pp. 409–426.

[25] Mary Ann Branch, Thomas F. Coleman, and Yuying Li. "A Subspace, Interior, and Conjugate Gradient Method for Large-Scale Bound-Constrained Minimization Problems". In: *SIAM Journal on Scientific Computing* 21.1 (Jan. 1999), pp. 1–23.

[26] Aymeric Spiga et al. "Rocket dust storms and detached dust layers in the Martian atmosphere". en. In: *Journal of Geophysical Research: Planets* 118.4 (2013), pp. 746–767.

[27] D. M. Kass et al. "Interannual similarity in the Martian atmosphere during the dust storm season". en. In: *Geophysical Research Letters* 43.12 (2016), pp. 6111–6118.

[28] Michael D. Smith. "THEMIS observations of Mars aerosol optical depth from 2002–2008". en. In: *Icarus* 202.2 (Aug. 2009), pp. 444–452.